RSC Advances

ROYAL SOCIETY OF CHEMISTRY

www.rsc.org/advances

RSC Advances

RSCPublishing

ARTICLE

High-efficiency water oxidation and energy storage utilizing various reversible redox mediators under visible light over surface-modified WO_3

Cite this: DOI: 10.1039/xoxxoooooox

Received ooth January 2012,
Accepted ooth January 2012

DOI: 10.1039/xoxxoooooox

www.rsc.org/

Yugo Miseki* and Kazuhiro Sayama*

Tungsten trioxide (WO_3) powder, treated with various metal salt solutions, was used for the photocatalytic oxidation of water into O_2; the reaction was accompanied by the reduction of various redox oxidants. The photocatalytic activity of WO_3 was remarkably improved by thermal treatment with alkali metal and silver salt aqueous solutions. Cs-treated WO_3 showed the highest activity. The WO_3 particles were covered with a very thin layer of a cesium tungstate species, and the ion-exchangeable sites on the WO_3 surface were formed by Cs-treatment. The activity of Cs-treated WO_3 was further improved by ion exchange of H^+ and Fe^{2+} ions and was 24 times higher than the activity of WO_3 without treatment. All methods of O_2 evolution using IO_3^- and VO_2^+ on WO_3 were also significantly improved with Cs-treatment, which suppressed the reverse reaction of the oxidation of the various redox reductants. The optimized WO_3 in $Fe(ClO_4)_3$ aqueous solution had a high quantum yield (31% at 420 nm) and solar-to-chemical energy conversion efficiency (0.38%).

Introduction

Water splitting by photocatalysis has been studied as an ideal candidate for solar energy conversion and storage.[1-7] Water reduction and oxidation must be separately induced on a semiconductor particle in conventional one-electron excitation systems. Therefore, a photocatalyst material should have a band structure that can thermodynamically induce water-oxidation and water-reduction reactions (conduction band potential < 0 V vs. RHE, valence band potential > +1.23 V vs. RHE).[4] Moreover, it should be stable against photo-generated holes because some semiconductor materials can oxidize themselves by such holes in the absence of a reducing agent. Therefore, there are very few reports on direct water splitting by visible light, even though visible-light photocatalysts are necessary for developing highly efficient solar-light-driven water splitting.[8,9] We first reported the stoichiometric decomposition of water into H_2 and O_2 using only visible light ($\lambda > 420$ nm) via a two-photon excitation system (Z-scheme system) that mimicked natural photosynthesis, which is a similar two-photon energy conversion system.[10]

$$n\mathrm{Ox} + 2\mathrm{H_2O} \rightarrow n\mathrm{Red} + 4\mathrm{H^+} + \mathrm{O_2}$$
$$\Delta G\ (\mathrm{eV}) = +1.23 - E_{ox/red}\ (-0.059\ \mathrm{pH}) \quad \text{(Eqn. 1)}$$

$$n\mathrm{Red} + 4\mathrm{H^+} \rightarrow n\mathrm{Ox} + 2\mathrm{H_2}$$
$$\Delta G\ (\mathrm{eV}) = +E_{ox/red}\ (+0.059\ \mathrm{pH}) \quad \text{(Eqn. 2)}$$

$$2\mathrm{H_2O} \rightarrow 2\mathrm{H_2} + \mathrm{O_2}$$
$$\Delta G\ (\mathrm{eV}) = +1.23 \quad \text{(Eqn. 3)}$$

In these equations, Ox is the redox oxidant, Red is the redox reductant, $E_{ox/red}$ is the redox potential of the redox reagent, ΔG is the Gibbs free energy change, and 0.059 pH is the term added when the redox potential is pH independent.

In this system, water is decomposed via the combination of two photocatalytic reactions (Eqn. 1 and 2), which proceed more easily thermodynamically compared to direct water splitting. Therefore, this system can potentially use a semiconductor for water-reduction or water-oxidation potential of one side of the reaction, suggesting that the potentials of the conduction and valence bands are not restricted compared to the conventional one-photon excitation system. Moreover, separation of the evolved H_2 and O_2 is possible. Visible-light-responsive systems combined with various photocatalysts and redox reagents for water splitting have been widely reported recently (Fig. 1).[11-20]

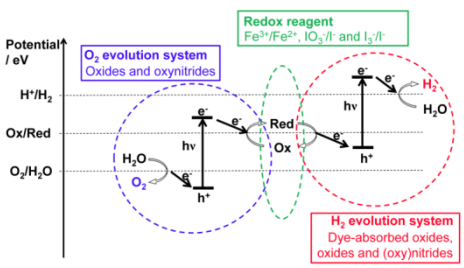

Figure 1. Two-photon excitation (Z-scheme) system combined with various types of photocatalysts and redox reagents.

However, the efficiency of these systems remains low. Therefore, techniques that can improve the quantum efficiency (QE) of the

photocatalytic reactions for Eqn. 1 and 2 are important for high-efficiency water splitting. I_3^-/I^- (+0.55 V vs. RHE),[17,19] Fe^{3+}/Fe^{2+} (+0.77 V vs. RHE),[21,22] VO_2^+/VO^{2+} (+1.00 V vs. RHE),[23] and IO_3^-/I^- (+1.09 V vs. RHE)[10,12-15,18,24] have been reported as reversible redox ions that utilize Eqn. 1 and 2. With respect to stability, cost, and redox potential, Fe^{3+}/Fe^{2+} is an excellent redox mediator. It was reported that the Fe^{2+} ion was produced in relatively high QE over a WO_3 photocatalyst under visible light using organic compounds as sacrificial electron donors.[25] However, the photocatalytic activity of Fe^{2+} production without sacrificial electron donors for Eqn. 2 was very low (QE < 0.4% at 405 nm).[20,21,26,27] We reported in a short communication that the oxidation of water into O_2 over WO_3 in a $FeCl_3$ aqueous solution was improved by Cs-treatment;[20] however, the efficiency was low (quantum yield (QE) = 19% at 420 nm) and the mechanism was unclear. One of the reasons for low efficiency is that the reverse reactions easily proceed in semiconductor photocatalysts, as shown in Fig. 2.[7] Ideally, only the redox oxidant (Ox) reduction (shown in Fig. 2 as a solid line) and water oxidation selectively proceed in an O_2-evolution photocatalyst. However, a redox reductant (Red) is accumulated in the reactant solution as the reaction proceeds. As a result, Red oxidation (shown in Fig. 2 as a broken line) preferentially proceeds instead of water oxidation because of the thermodynamic advantage. Consequently, the apparent reaction efficiency decreases significantly. Therefore, it is important to develop techniques that suppress this undesirable back reaction. In this study, we investigated the oxidation and reduction properties of a WO_3 photocatalyst systematically treated with various ions using various redox mediators. We discovered that the undesirable back reactions of the Reds and holes were significantly suppressed by the presence of a thin cesium tungstate layer on the WO_3 surface. Optimized WO_3 in an aqueous $Fe(ClO_4)_3$ solution showed a very high QE (31% at 420 nm) and solar-to-chemical energy conversion efficiency (0.38%).

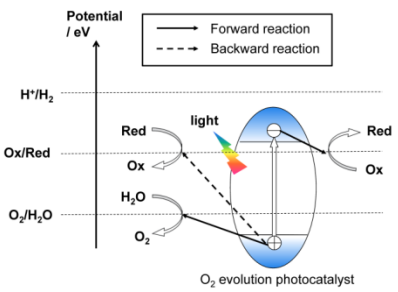

Figure 2. Forward and back reactions that proceed in water oxidation and redox oxidant reduction.

Experimental

Preparation

WO_3 (Kojundo Chemical Laboratory Co., Ltd.) powder was used as the starting material. The WO_3 powder was first thermally treated in air at 973 K to improve its crystallinity. Some metal salts such as alkali, alkaline earth, and transition-metal salts were used for surface modification of the WO_3 photocatalyst Surface modifications were conducted by an impregnation method. 0.5 g of WO_3 powder was dispersed in 0.5 mL of 4.3–215 mM metal salt solution, and then the slurry was evaporated to dryness followed by thermal treatment at 373–973 K for 10–600 min. Then, these catalysts were stirred in H_2SO_4 or $FeSO_4$ aqueous solutions for 30 min for ion exchange, if necessary. TiO_2 powder (rutile, Toho Titanium Co., Ltd.) was used as the photocatalyst based on literature.[28] $BiVO_4$ was prepared from Bi_2O_3 and V_2O_5 in a 0.75M HNO_3 aqueous solution at room temperature according to literature.[29]

Characterization

Diffuse reflection spectra were obtained using a UV–vis–NIR spectrometer (JASCO Corporation, UbestV-570). Phase purity of the obtained modified WO_3 powder was confirmed by X-ray diffraction (PANalytical, EMPYREAN) and Raman spectroscopy (JASCO Corporation, NRS-1000, excitation at 532 nm). X-ray photoelectron spectra were obtained using an X-ray photoelectron spectrometer (Ulvac-Phi, XPS-1800). WO_3 particles were observed using scanning electron microscopy (SEM, Hitachi, Ltd., S-4800) and transmission electron microscopy (TEM, Hitachi High-Technologies Corporation., H-9000NAR). The particles for TEM samples were sliced into thin sections by Focused ion beam method. The adsorption amounts of Fe^{2+} and Fe^{3+} on various WO_3 catalysts were determined by color reactions using phenanthroline and chloride ions, respectively.

Photocatalytic Reactions

Photocatalytic reactions were performed in a side-window cell made of Pyrex connected to a gas-closed circulation system. A 300-W Xe illuminator (ILC Technology, Inc., CERMAX-LX300) attached to a cut-off filter (HOYA Corporation, L42) was employed for visible-light irradiation. The photocatalyst powder (0.4 g) was dispersed in the Fe^{3+} aqueous solution (300 mL) using a magnetic stirrer. The initial pH in the Fe^{3+} solution was adjusted to 2.3 for all photocatalytic reactions. An aqueous VO_2^+ solution (pH 0.7) was prepared by dissolving V_2O_5 in a 1-M H_2SO_4 aqueous solution. An aqueous IO_3^- solution (pH 6.5) was prepared by dissolving $NaIO_3$ in pure water. For the reaction where the IO_3^- ion was used as the redox mediator, the Pt cocatalyst was loaded on the WO_3 photocatalyst according to a literature method.[10] NaI, $VOSO_4$, and $FeSO_4$ were dissolved in the reactant solutions as Red sources, if necessary. The amount of the evolved O_2 was determined using on-line gas chromatography (Shimadzu Corporation, MS-5A column, TCD, Ar carrier). The apparent QE was measured using monochromatic light through a bandpass filter. The number of incident photons was determined using a Si photodiode proofread by NMIJ (National Metrology Institute of Japan). The solar-to-chemical energy-conversion efficiency (η_{sun}) was measured using a solar simulator (Sanei Denki Co., adjusted to AM 1.5 and 1 SUN by a spectroradiometer). Solar-energy-conversion efficiency was defined by the following equation (4).

Solar-energy conversion (%) = [Output energy as Fe(II) ions]/[Energy of incident solar light] × 100 = [Gibbs free energy change, ΔG_{298}^0] ×[Rate of O_2 evolution × 2]/[Energy of incident solar light] × 100 (Eqn. 4)

Preparation and photoelectrochemical measurement of WO_3 photoelectrodes

A WO_3 electrode (sputtering film on conducting glass purchased from NSG Techno-Research Co. Ltd., thickness: ~1 μm, aggregation of the particles: ~50 nm) was calcined at 923 K for 30 min. A Cs_2CO_3 aqueous solution was dropped onto the WO_3 electrode, which was then calcined at 773 K for 10 min. In addition, the WO_3 electrode was soaked in H_2SO_4 or $FeSO_4$ aqueous solution for 30 min. The photoelectrochemical measurements were performed using a potentiostat (BAS Co.) and a Pyrex glass cell. A Pt wire and Ag/AgCl electrode were used as the counter and reference electrodes, respectively.

Results and Discussion

Effect of thermal treatment using various metal aqueous solutions for WO_3 photocatalyst on photocatalytic water oxidation accompanied by Fe^{3+} reduction

Fig. 3 shows the reaction rates for water oxidation into O_2 using WO_3 photocatalysts treated with various metal aqueous solutions.

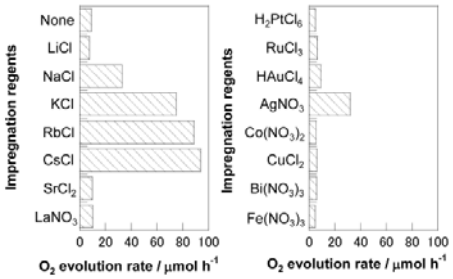

Figure 3. Water-oxidation reaction rates of WO_3 photocatalysts treated with various metal aqueous solutions. Impregnation reagent amount: 1 mol% for WO_3. Impregnation condition: 773 K for 30 min. Catalyst: 0.4 g, reactant solution: 300 mL of 2 mM $Fe_2(SO_4)_3$, light source: 300 W Xe-arc lamp (λ > 420 nm), reaction cell: side-irradiation cell. Initial pH of reactant solution was always adjusted to be 2.3 using sulfuric acid. WO_3 was calcined at 973 K for 2 h in air as a pretreatment.

Native WO_3 showed little activity for water oxidation, as reported previously.[20,21,26,27] The activity of WO_3 was remarkably improved by thermal treatment at 773 K using MCl (M = Na, K, Rb, and Cs) and $AgNO_3$ aqueous solution. WO_3 treated with cesium aqueous solution (Cs-WO_3) showed the best activity. The X-ray diffraction patterns, Raman spectra, and diffuse reflection spectra (DRS) of the WO_3 photocatalysts barely changed with the Cs-WO_3 (Fig. S1(I)–(III)), suggesting that the bulk of WO_3 was unchanged. On the other hand, Cs^+ was detected on Cs-WO_3 by XPS measurement even after washing thoroughly with pure water (Table 1). Cs_2CO_3 (or CsOH) is usually readily soluble in water. Therefore, it was determined that a water-insoluble Cs^+ species formed on the WO_3 surface. The elemental ratio of Cs/W estimated by X-ray photoelectron spectroscopy (XPS) on the Cs-WO_3 surface after calcination at 773 K (0.22–0.25) had almost the same value as that found on Cs-WO_3 without calcination (0.19–0.21). The radius of Cs^+ is too large for it to penetrate the bulk. Thus, most of the Cs^+ is likely present on the WO_3 surface, which is within the detection depth of XPS (ca. 2 nm). Fig. 4 shows the SEM images of WO_3, with and without Cs-modification.

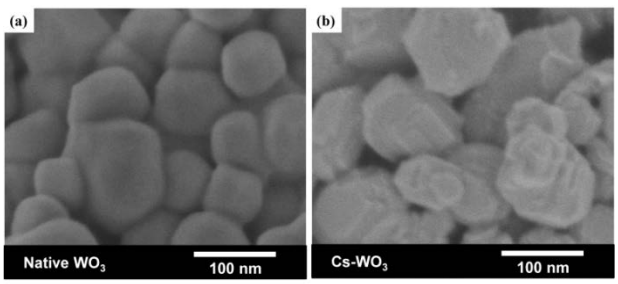

Figure 4. Scanning electron microscopy images of (a) WO_3 and (b) Cs-WO_3 photocatalysts. Cs amount: 1 mol% for WO_3.

A nanostep structure with plane terraces formed on the WO_3 particles with Cs-modification; however, the native WO_3 particles without any treatment had characterless and roundish surfaces, suggesting that the surface of WO_3 was reconstructed by the Cs-modification. It has been reported that a similar surface nanostep structure forms on $NaTaO_3$ particles by doping with La or alkaline earth metals, and this surface structure promotes the charge separation of photo-generated electrons and holes, resulting in increased activity for water splitting compared to the activity on nondoped $NaTaO_3$.[30,31] Therefore, there is a possibility that the high activity of Cs-WO_3 might result because of this surface morphology change. Fig. 5 shows the TEM images of WO_3 and Cs-WO_3.

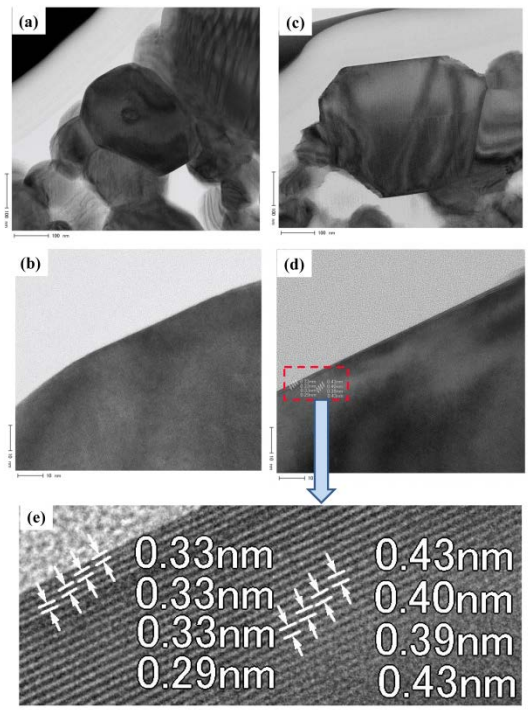

Figure 5. Transmission electron microscopy images of (a)-(b) WO_3 and (c)-(e) Cs-WO_3 photocatalysts. Cs amount: 1 mol% for WO_3.

The entire Cs-WO_3 particle was covered by thin compound layers (ca. 2 nm) with different lattice spacing compared to the WO_3 bulk; however such a thin film was not observed on the WO_3 surface. The lattice spacing of the thin surface layers is smaller than that of the WO_3 bulk, despite the fact that the ion radius of Cs^+ (1.67 Å) is much large than that of W^{6+} (0.60 Å). Therefore, it was determined that the crystal structure of the surface layers became different from the ReO_3 structure (WO_3 bulk) by incorporating Cs^+. From the above results, it was surmised that the high activation of the WO_3 photocatalyst treated with Cs^+ was derived from the reconstructed surface structure and/or the presence of a water-insoluble thin film of cesium tungstate on the WO_3 surface.

Fig. 6 shows the time course of O_2 evolution over WO_3 photocatalysts, with and without Cs-treatment. Cs-WO_3 showed the highest activity when an aqueous CsCl solution (2.2 mol % for WO_3) was impregnated at 773 K for 30 min. The total amount of O_2

gas reached ca. 300 μmol over Cs-WO_3, thus agreeing with the stoichiometric amount expected from Fe^{3+} (1200 μmol) in the solution. The stoichiometric amount of Fe^{2+} was detected in the solution after the photoreaction; Fe^{3+} was not detected after the photoreaction. The activity of the second run over Cs-WO_3 (c) was much higher than that of the first run (b), though an improvement in the second run was not observed for WO_3 with no Cs-treatment. Therefore, it was determined that the further improvement was derived from the changing surface condition of the Cs-WO_3 photocatalyst during the photoreaction.

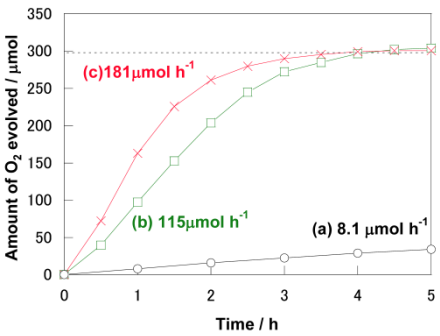

Figure 6. Photocatalytic O_2 evolution over (a) WO_3 without Cs-treatment, (b) Cs-WO_3 (1st run), and (c) Cs-WO_3 (2nd run) under visible-light irradiation. Cs amount: 2.2 mol% for WO_3. Broken line shows upper limit of O_2 evolution expected from the amount of Fe^{3+} (1200 μmol) added to solutions. Second run reaction was performed by exchanging reactant solution of 1st run with fresh $Fe_2(SO_4)_3$ aqueous solution. Catalyst: 0.4 g, reactant solution: 300 mL of 2 mM $Fe_2(SO_4)_3$, light source: 300 W Xe-arc lamp (λ > 420 nm), reaction cell: side-irradiation cell. Initial pH of reactant solution was always adjusted to 2.3 using sulfuric acid.

Analyses of detail surface conditions of Cs-WO_3 using XPS and DRS measurements

Some alkali complex oxides possessing layered or tunnel structures have ion-exchange abilities. The ratio of Cs/W based on the XPS decreased when the stirring treatment with 1M H_2SO_4 solution was performed for Cs-WO_3. Moreover, the Na 1s signal was detected on the Cs-WO_3 surface after performing stirring treatment with 1M NaCl solution; however, there was no signal derived from Na^+ for native WO_3 (Fig. S2). These results suggest that the cesium tungstate species of the thin WO_3 surface layers have an ion-exchange ability and can be exchanged for H^+ and Na^+. As for the ion-exchange candidates, H^+, Fe^{2+}, and Fe^{3+} ions are present in the reactant solution. Table 1 shows the effects of ion-exchange treatments for Cs-WO_3 and WO_3 on photocatalytic activities. The photocatalytic activities of native WO_3 had no practical impact on the ion-exchange treatments using various aqueous solutions because it has no ion-exchange ability. On the other hand, ion-exchanged Cs-WO_3 with 1M H_2SO_4 solution (H-Cs-WO_3) has a higher activity compared to Cs-WO_3 washed with pure water. Here, the activity of H-Cs-WO_3 drastically decreased (from 156 to 27 μmol h^{-1}) when H-Cs-WO_3 underwent thermal treatment at 673 K for 30 min. It is likely that this inactivation was related to the extinction of H^+-exchanged sites via a dehydration reaction. It was noted that the surface structure with nanostep and plane terrace on H-Cs-WO_3, as shown in Fig. 4, remained after this thermal treatment (Fig. S3). Therefore, the high activation of WO_3 by Cs-modification is mainly caused by the introduction of ion-exchange sites on the WO_3 surface, and the contribution of the surface structure with nanostep and plane terrace is not very large.

Table 1. Effect of ion-exchange treatment of Cs-WO_3 and WO_3 on photocatalytic activities for water oxidation accompanied with Fe^{3+} reduction.

Catalyst	Ion-exchange treatment solution[b]	Surface atom ratio (W : Cs : Fe)	O_2-evolution rate / μmol h^{-1}
Cs-WO_3[a]	Pure water	1 : 0.25 : 0	118
Cs-WO_3[a]	H_2SO_4	1 : 0.16 : 0	156 (27)[c]
Cs-WO_3[a]	$Fe_2(SO_4)_3$	1 : 0.12 : 0.14	116
Cs-WO_3[a]	$FeSO_4$	1 : 0.14 : 0.02	200
WO_3	Pure water	1 : 0 : 0	8.1
WO_3	H_2SO_4	1 : 0 : 0	7.5
WO_3	$Fe_2(SO_4)_3$	1 : 0 : 0.10	8.7
WO_3	$FeSO_4$	1 : 0 : 0.02	8.4

Catalyst: 0.4 g, reactant solution: 300 mL of 2 mM $Fe_2(SO_4)_3$, light source: 300 W Xe-lamp (L42). [a]Cs amount: 2.2 mol% for WO_3. [b]Ion exchange was conducted for 30 min. [c]Activity of calcined catalyst at 673 K for 30 min after H^+ exchange.

We also found that the photocatalytic activity of H-Cs-WO_3 was further improved from 156 to 200 μmol h^{-1} by ion exchange for the Fe^{2+} ion (Fe-H-Cs-WO_3); however, the activity of H-Cs-WO_3 was unchanged after stirring in a Fe^{3+} solution, as shown in Table 1. The color of the Cs-WO_3 powder also changed only after stirring in the Fe^{2+} solution. Fig. 7 shows the DRS spectra of ion-exchanged Cs-WO_3 with Fe^{2+} and Fe^{3+} aqueous solutions. The specific absorption band developed in the wavelength range 450–600 nm on the Cs-WO_3 photocatalyst after the stirring treatment with the Fe^{2+} solution, but not with the Fe^{3+} solution. Therefore, it was determined that this specific absorption was derived from the Fe^{2+} ion incorporated on the WO_3 surface by an ion-exchange reaction. Cs^+- and H^+-ion-exchanged sites on the WO_3 surface may not directly replace the Fe^{3+} ion because of the difference in the atomic value. Consequently, experiments indicated that the ion-exchange sites formed on the cesium tungstate species on the thin WO_3 surface layers, and Cs^+ ions were exchanged for H^+ and Fe^{2+}, improving the photocatalytic activity.

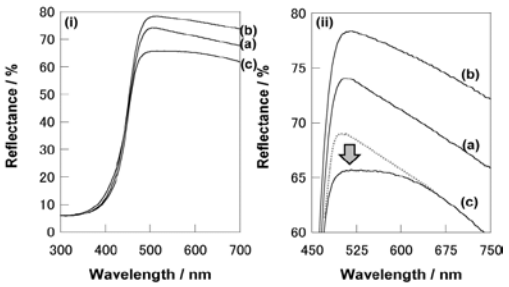

Figure 7. (i) Reflection spectra of Cs-WO_3. (a) Powder dispersion in 10 mM H_2SO_4 aq. sol., (b) 4 mM Fe^{3+} sol., and (c) 4 mM Fe^{2+} aq. sol., (ii) magnification of (i). Cs amount: 1 mol% for WO_3.

It was noted that the Fe/W ratios on WO_3 and Cs-WO_3 treated with Fe^{3+} solution were higher than those treated with Fe^{2+} solution

(Table 1). This result also indicates that the characteristic changes in the powder color and photocatalytic ability were caused by a small amount of Fe^{2+} incorporating in the ion-exchange sites, and not by Fe^{3+} adsorption on the WO_3 surface. Fe-H-Cs-WO_3 showed no activity when the irradiation wavelength was longer than 500 nm. Therefore, the absorption band derived from the Fe^{2+} ion is not available for the water-oxidation reaction in the presence of the Fe^{3+} ion. Here, we examined the ion-exchange effects for H^+ and Fe^{2+} over M-WO_3 (M = Na, K, Rb, and Ag) on photocatalytic activities. The activities of all WO_3 photocatalysts improved with ion-exchange treatments (Fig. S4). Therefore, it was concluded that the high activation of M-WO_3 (M = Na, K, Rb, and Ag) photocatalysts is derived from a mechanism similar to Cs-WO_3 and is based on the ion-exchange ability.

Effects of condition of reactant solution over Cs-WO_3 photocatalyst on photocatalytic water oxidation in the presence of Fe^{3+} ions.

In the case of Fe^{3+} reduction, Fe^{3+} ions must preferentially arrive at the photocatalyst surface and easily receive the photo-generated electrons from the photocatalyst.[28] Fe^{3+} ions form various types of complex ions, depending on the coexisting anion species.[32-34] The adsorption and reaction behaviors of the Fe^{3+} ion are changed by the state of the Fe^{3+} complex ion. Therefore, it is likely that the state of a Fe^{3+} complex ion affects the photocatalytic activity for Fe^{3+} reduction. Table 2 shows the photocatalytic O_2-evolution activity over Fe-H-Cs-WO_3 under various reactant solution conditions. The activities strongly depended on the type of iron source. Fe-H-Cs-WO_3 showed the highest activity in an aqueous $Fe(ClO_4)_3$ solution. There was a poor correlation between the reaction rate and the adsorption amount of Fe^{3+} ions. Therefore, it is likely that there are other factors affecting the photocatalytic activities. This tendency of the coexisting anion species was also observed in the case of other photocatalysts, native WO_3, $BiVO_4$, and TiO_2 (Table 3). The photocatalytic activities of WO_3, $BiVO_4$, and TiO_2 using the $Fe(ClO_4)_3$ solution were 4.4, 4.7, and 12 times higher than those using the $Fe_2(SO_4)_3$ solution.

Table 2. Photocatalytic O_2 evolution over Fe-H-Cs-WO_3 in various reactant solution conditions.

Catalyst	Fe^{3+} source	Adsorption amount / μmol g^{-1}		O_2-evolution rate / μmol h^{-1}
		Fe^{3+}	Fe^{2+}	
Cs-WO_3[a]	$Fe_2(SO_4)_3$	16	nd.	200
Cs-WO_3[a]	$FeCl_3$	14	nd.	241
Cs-WO_3[a]	$Fe(NO_3)_3$	—	—	290
Cs-WO_3[a]	$Fe(ClO_4)_3$	18	nd.	297

Catalyst: 0.4 g, reactant solution: 300 mL of 2 mM Fe(III), light source: 300 W Xe-lamp (L42). Nd, not detected. [a]Cs amount: 2.2 mol% for WO_3.

Table 3. Effect of types of Fe^{3+} solution over TiO_2, WO_3, and $BiVO_4$ photocatalyst on reaction rates for water oxidation.

Catalyst	Fe^{3+} source	pH adjuster[a]	Irradiation wavelength	O_2-evolution rate / μmol h^{-1}
TiO_2	$Fe_2(SO_4)_3$	H_2SO_4	λ > 300 nm	30
WO_3	$Fe_2(SO_4)_3$	H_2SO_4	λ > 420 nm	8.1
$BiVO_4$	$Fe_2(SO_4)_3$	H_2SO_4	λ > 420 nm	47
TiO_2	$Fe(ClO_4)_3$	$HClO_4$	λ > 300 nm	370
WO_3	$Fe(ClO_4)_3$	$HClO_4$	λ > 420 nm	35
$BiVO_4$	$Fe(ClO_4)_3$	$HClO_4$	λ > 420 nm	221

Catalyst: 0.4 g, reactant solution: 300 mL of 2 mM Fe(III), light source: 300 W Xe-lamp. [a] Initial pH was always adjusted to 2.3.

The cyclic voltammetry (CV) profiles of various Fe^{3+} solutions changed depending on the type of iron solution (Fig. 8). The order of redox potentials estimated by the CVs was: SO_4^{2-} (+0.72 vs. RHE) < Cl^- (+0.77 vs. RHE) < NO_3^- = ClO_4^- (+0.79 vs. RHE). There was a good correlation between the redox potential and reaction rate. The negative shift of the redox potential shows that it is thermodynamically difficult to reduce the Fe^{3+} ion. On the other hand, the difference between the conduction band potentials of these photocatalysts (WO_3[35], $BiVO_4$[35], and TiO_2[36]) and the $Fe^{3+/2+}$ redox potential are estimated to be ca. 0.3, 0.7, and 0.8 V, respectively.

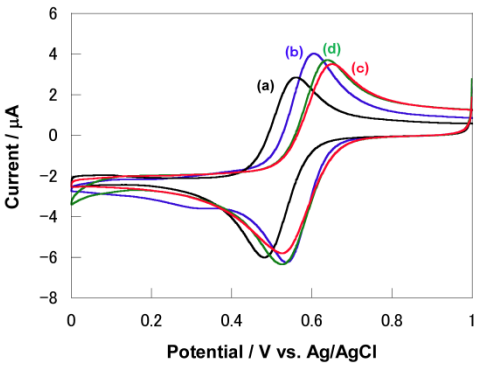

Figure 8. Cyclic voltammetry at Pt-electrode (SA: 0.01 cm^2) in (a) 2.0 mM $Fe_2(SO_4)_3$ in 0.1M Na_2SO_4, (b) 4.0 mM $FeCl_3$ in 0.1M NaCl, (c) 4.0 mM $Fe(NO_3)_3$ in 0.1M $NaNO_3$, and (d) 4.0 mM $Fe(ClO_4)_3$ in 0.1M $NaClO_4$. pH value of iron solutions was adjusted to 2.3 using (a) H_2SO_4, (b) HCl, (c) HNO_3, and (d) $HClO_4$. Scan rate: 5 mV s^{-1}.

There was no correlation between the improvement in the photocatalytic activity and the value of the potential difference. Therefore, we could not explain the photocatalytic behaviors using only the potential differences. Fe^{3+} ions in aqueous $Fe_2(SO_4)_3$ or $FeCl_3$ solutions mainly form $Fe(SO_4^{2-})_x(H_2O)_{6-x}$ or $Fe(Cl^-)_x(H_2O)_{6-x}$ and $Fe(H_2O)_6$ in aqueous $Fe(NO_3)_3$ and $Fe(ClO_4)_3$.[32-34] The difference of coordinate species for Fe^{3+} ions may affect the reducibility of Fe complex ions; it may be difficult to reduce the Fe^{3+} ion if SO_4^{2-} or Cl^- ions are introduced in the Fe^{3+} complex ions compared to only H_2O coordination. Therefore, it was concluded that the photocatalytic reaction rates were strongly affected by the coordination of the Fe^{3+} complex ion and thermodynamic reducibility of the Fe complex ions. Fig. 9 shows the action spectrum of water oxidation over a Fe-H-Cs-WO_3 photocatalyst in $Fe(ClO_4)_3$. The apparent QE at 420 nm was 31%. This is the highest value

among all the photocatalysts using reversible redox mediators under visible light. It was confirmed that the QE estimated by the Fe^{2+}-production rate had the same value as that of the efficiency estimated by the O_2-production rate. The QE at 365 nm was 21%. The Fe^{3+} solution shows a strong absorption in the UV light region (Fig 9(c)).

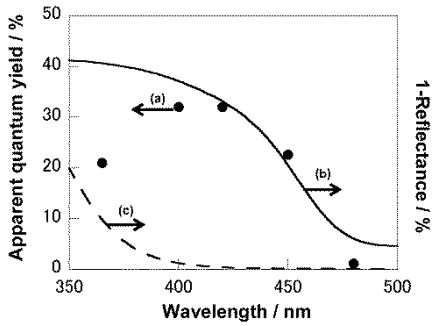

Figure 9. (a) Action spectrum of water oxidation in the presence of Fe^{3+} ions. Absorbance spectra of (b) Cs-WO_3 photocatalyst and (c) $Fe(ClO_4)_3$ solution.

Therefore, it is likely that the QE was low because of the light-shield effects of the Fe^{3+} reactant solution. Fig. 10 shows the time course of O_2 evolution over a Fe-H-Cs-WO_3 photocatalyst in $Fe(ClO_4)_3$ when a solar simulator (AM 1.5) is used as the light source.

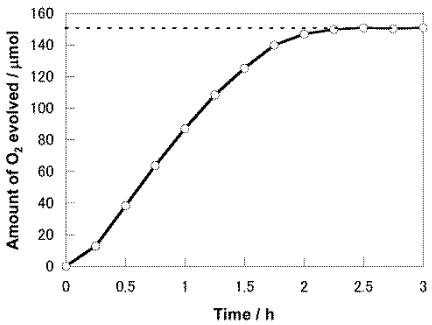

Figure 10. Time course of photocatalytic water oxidation accompanied with Fe^{3+} reduction using solar simulator (AM 1.5). Broken line shows upper limit of O_2 evolution expected from the amount of Fe^{3+} (600 μmol) added to solution. Cs-WO_3: 0.4 g, reactant solution: 300 mL of 2 mM $Fe(ClO_4)_3$, reaction cell: side-irradiation cell. Initial pH of reactant solution was always adjusted to 2.3 using perchloric acid.

O_2-evolution rate at Fe^{3+}/Fe^{2+} = 1 was 94 μmol h^{-1} (irradiation area: 9 cm^2). The water oxidation reaction accompanied by Fe^{3+} reduction is the energy-storage reaction shown in Eqn. 5. The solar-to-chemical energy-conversion efficiency (η_{sun}) was estimated to be 0.38%. This is also the best value among all the photocatalysts using reversible redox mediators.

$$2Fe^{3+} + H_2O \rightarrow 2Fe^{2+} + 2H^+ + 1/2O_2 \ (pH = 2)$$
$$\Delta G = 66.1 \text{ kJ} \qquad \text{(Eqn. 5)}$$

Mechanism of activation by Cs treatment

We investigated the photoelectrochemical performance of WO_3 electrodes to elucidate the role of surface treatment on WO_3 photocatalysts because reductive and oxidative reactions can be individually evaluated by photoelectrochemical methods. Table 4 shows the O_2-production photocurrent at 0.8 V vs. RHE and Fe-reduction current at 0.45 V vs. RHE for WO_3 electrodes with and without surface treatment, respectively.

Table 4. O_2-production photocurrent and Fe^{3+}-reduction current over various surface-treated WO_3 photoelectrodes.

Photoelectrodes	O_2-production photocurrent at 1.0 V / mA	Fe^{3+}-reduction current at 0.4 V / mA
WO_3	0.11	0.45
Fe-WO_3	0.12	0.47
H-Cs-WO_3	0.20	0.49
Fe-H-Cs-WO_3	0.20	0.55

The O_2-production photocurrent of the H-Cs-WO_3 electrode was much higher than that of the WO_3 electrode without treatment, indicating that water oxidation is promoted on the H-Cs-WO_3 surface; further improvement by the partial ion exchange for Fe^{2+} was very small. On the other hand, the Fe^{3+}-reduction current of the Fe-H-Cs-WO_3 electrode was higher than that of the other electrodes, suggesting that Fe^{3+} reduction is promoted on the Fe-H-Cs-WO_3 surface. The H^+-exchanged site would be strongly adsorbed with water as H_3O^+, which is suitable for the H_2O oxidation. On the other hands, the Fe^{2+}-exchange site may act as the effective reduction site of Fe^{3+} adsorbed on the outer surface of the photocatalyst, because the electron transfer between the same element ions (Fe^{2+} and Fe^{3+}) is ideal. Consequently, both reduction and oxidation abilities of WO_3 improved at different sites formed by Cs-modification and followed by ion exchange for Fe^{2+} and H^+ ions, resulting in the surface-modified WO_3 photocatalyst showing remarkably high activity.

The suppression of the reverse reaction between the photo-generated holes and Fe^{2+} ions as shown in Fig. 2 is important for realizing highly efficient water oxidation. Fig. 11(a,b) shows the influence of the concentration of coexisting Fe^{2+} ions with 2mM of Fe^{3+} ions over the WO_3 photocatalyst, with and without surface modification, on the photocatalytic activity for water oxidation into O_2. The activity of native WO_3 decreased when 0.5 mM of Fe^{2+} ions coexisted in the reactant solution. This indicates that the Fe^{2+} ion is easily oxidized compared to water on a normal WO_3 surface. On the other hand, the activity of the Fe-H-Cs-WO_3 photocatalyst was unaffected by the concentration of the Fe^{2+} ion. This suggested that surface modification improves the oxidation and reduction abilities of WO_3; it also improves the suppression effect on the undesirable reaction between the photo-generated holes and Fe^{2+} ions.

Fig. 11(c–f) shows the suppression effect for WO_3 photocatalysts with and without surface modification on the undesirable reaction when other reversible redox mediators are used (VO_2^+/VO^{2+}: +1.00 vs. RHE and IO_3^-/I^-: +1.09 vs. RHE). The photocatalytic activities of Pt/WO_3 and WO_3 in the presence of IO_3^- and VO_2^+ ions for O_2 evolution remarkably improved (3.5 and 7.3 times, respectively) with surface modification. Among the reactions using different redox mediators, water oxidation to O_2 gas was the common reaction, suggesting that an excellent water-oxidation site is probably formed on the surface-modified WO_3 photocatalyst. Interestingly, the undesirable reactions were also effectively suppressed over the Fe-H-Cs-WO_3 photocatalyst, while the activity of native WO_3

drastically decreased when 0.5 mM of I^- or VO^{2+} ions were also present in the reactant solution. Therefore, an excellent suppression effect for the undesirable reaction between the photo-generated holes and Red was obtained, regardless of the type of redox reagent. Thus, this ideal reaction selectivity arose because of the suppression of the undesirable reaction between the photo-generated holes and various Reds and the construction of an effective site that can induce only water oxidation.

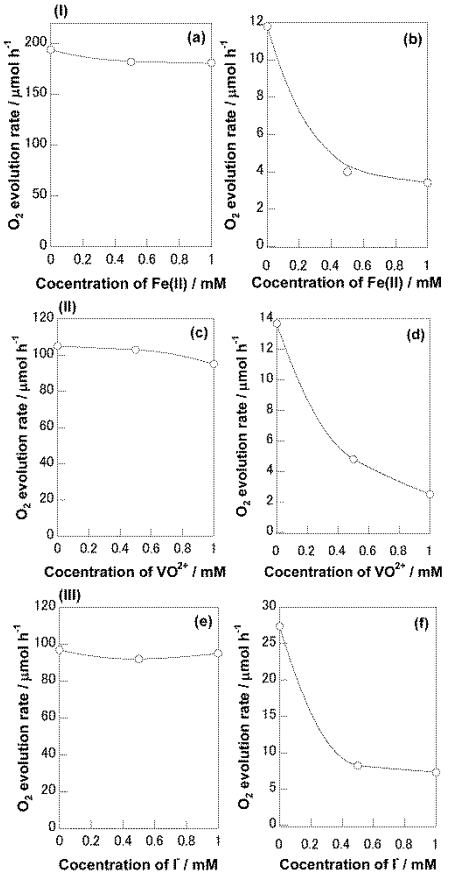

Figure 11. Effect of concentration of (I) Fe^{2+}, (II) VO^{2+}, and (III) I^- ions over WO_3 photocatalyst (a), (c), and (e) with and (b), (d), and (f) without surface ion-exchange sites on photocatalytic reaction rates for water oxidation in the presence of (I) Fe^{3+}, (II) VO_2^+, and (III) IO_3^- ions. In case of reaction using IO_3^- ion as redox mediator, Pt cocatalyst was loaded on WO_3 photocatalyst.

According to the results mentioned above, a few layers of cesium tungsten species initially formed on the WO_3 surface by thermal treatment using a cesium aqueous solution. Cs^+ sites in cesium tungsten species have ion-exchange ability, and Cs^+ easily exchanged for H^+ and Fe^{2+} in acidic Fe^{2+} solutions. Electrochemical technique showed that the H^+-exchange site promotes water oxidation, and the Fe^{2+}-exchange site promotes Fe^{3+} reduction. Moreover, the photo-generated hole can selectively oxidize water to O_2 even when various Reds were present. Consequently, the surface-modified WO_3 photocatalyst showed remarkably high activity for water oxidation (Fig. 12). A redox potential is usually more negative than the water oxidation potential (+1.23 vs. RHE) in the case of water oxidation with a positive Gibbs free energy change. Therefore, the Red is easily oxidized compared to water, even though this reaction is undesirable. In this study, the undesirable reaction was effectively suppressed on a Fe-H-Cs-WO_3 photocatalyst. These results provide a promising route for improving various photocatalytic water-splitting techniques such as the Z-scheme system, photocatalysis-electrolysis system,[20] and Fe^{2+} ion fuel cells.[36,37]

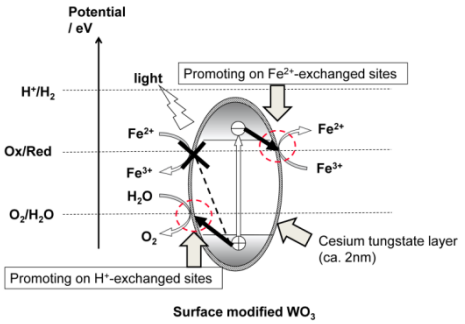

Figure 12. Description of highly activated WO_3 surface.

Conclusions

WO_3 powders modified with various metal salt solutions were studied as photocatalysts for the oxidation of water to O_2 gas in an aqueous Fe^{3+} solution under visible light ($\lambda > 420$ nm). The activity of WO_3 was remarkably improved by thermal treatment at 773 K using MCl (M = Na, K, Rb, and Cs) and a $AgNO_3$ aqueous solution. WO_3 treated using a cesium aqueous solution had the highest activity. WO_3 particles were covered with a very thin layer of cesium tungstate species, which had a different structure from the WO_3 bulk. It was observed that the Cs^+ site of the cesium tungstate species on WO_3 had an ion-exchange ability, and the photocatalytic performances of the WO_3 photocatalyst were further improved by the ion-exchange treatment with H^+ and Fe^{2+} ions. The photocatalytic activity for water oxidation in the presence of Fe^{3+} ions was strongly dependent on the types of Fe^{3+} solutions. The best activities were obtained in a $Fe(ClO_4)_3$ aqueous solution over Cs-treated WO_3 and various other photocatalysts. The apparent QE at 420 nm and solar-to-chemical energy-conversion efficiency over Cs-treated WO_3 were 31% and 0.38%, respectively. These values are the best among the photocatalysts using various reversible redox mediators under visible light. Electrochemical analyses suggested that Fe^{2+}- and H^+-incorporated sites on the WO_3 surface promoted Fe^{3+} reduction and water oxidation, respectively. Moreover, the surface of the Fe-H-Cs-WO_3 photocatalyst had the ability to suppress undesirable reverse reactions between the photo-generated holes and Fe^{2+} ions. The improvement of the water oxidation and suppression of the reverse reaction were still obtained by Cs-treatment, even when other redox ions (IO_3^-/I^- and VO_2^+/VO^{2+}) were used. Therefore, the Cs-treated WO_3 has an excellent activity and a broad utility for the photocatalytic oxidation reaction of water to O_2 using various reversible redox mediators.

Acknowledgements

This research was supported by The Funding Program for Next Generation World-Leading Researchers (NEXT Program).

Notes and references

Energy Technology Research Institute, National Institute of Advanced Industrial Science and Technology (AIST),Central 5, 1-1-1 Higashi, Tsukuba, Ibaraki 305-8565. Fax: +81-29-861-4760; Tel: +81-29-861-4760; E-mail: yugo-miseki@aist.go.jp, k.sayama@aist.go.jp.

Electronic Supplementary Information (ESI) available: [details of any supplementary information available should be included here]. See DOI: 10.1039/b000000x/

1) 1 J. S. Lee, *Catal. Surv. Asia*, 2005, **9**, 217-227.
2) A. J. Esswein and D. G. Nocera, *Chem. Rev.*, 2007, **107**, 4022-4047.
3) F. E. Osterloh, *Chem. Mater.*, 2008, **20**, 35-54.
4) A. Kudo and Y. Miseki, *Chem. Soc. Rev.*, 2009, **38**, 253-278.
5) Y. Inoue, *Energy Environ. Sci.*, 2009, **2**, 364-386.
6) K. Maeda and K. Domen, *J. Phys. Chem. Lett.*, 2010, **1**, 2655-2661.
7) R. Abe, *Bull Chem. Soc. Jpn.*, 2011, **84**, 1000-1030.
8) K. Maeda, K. Teramura, D. Lu, T. Takata, N. Saito, Y. Inoue, and K. Domen, *Nature*, 2006, **440**, 295-295; K. Maeda, K. Teramura, and K. Domen, *J. Catal.*, 2008, **254**, 198-204.
9) Y. Lee, H. Terashita, Y. Shimodaira, K. Teramura, M. Hara, H. Kobayashi, K. Domen, and M. Yashima, *J. Phys. Chem. C*, 2007, **111**, 1042-1048.
10) K. Sayama, K. Mukasa, R. Abe, Y. Abe, and H. Arakawa, *Chem. Commun*., 2001, 2416-2417; K. Sayama, K. Mukasa, R. Abe, Y. Abe, and H. Arakawa, *J. Photochem. Photobiol. A: Chem.*, 2002, **148**, 71-77.
11) H. Kato, M. Hori, R. Konta, Y. Shimodaira, and A. Kudo, *Chem. Lett.*, 2004, **33**, 1348-1349; Y. Sasaki, A. Iwase, H. Kato, and A. Kudo, *J. Catal.*, 2008, **259**, 133-137.
12) R. Abe, T. Takata, H. Sugihara and K. Domen, *Chem. Commun*., 2005, 3829-3831; R. Abe, M. Higashi and K. Domen, *ChemSusChem*, 2011, **4**, 228-237.
13) M. Higashi, R. Abe, K. Teramura, T. Takata, B. Ohtani, and K. Domen, *Chem. Phys. Lett.*, 2008, **452**, 120-123; M. Higashi, R. Abe, T. Takata, and K. Domen, *Chem. Mater.*, 2009, **21**, 1543-1549.
14) M. Higashi, R. Abe, A. Ishikawa, T. Takata, B. Ohtani, and K. Domen, *Chem. Lett.*, 2008, **37**, 138-139.
15) K. Maeda, H. Terashima, K. Kase, M. Higashi, M. Tabata, and K. Domen, *Bull. Chem. Soc. Jpn*., 2008, **81**, 927-937; K. Maeda, M. Higashi, D. Lu, R. Abe, and K. Domen, *J. Am. Chem. Soc*., 2010, **132**, 5858-5868.
16) Y. Sasaki, H. Nemoto, K. Saito, and A. Kudo, *J. Phys. Chem. C*, 2009, **113**, 17536-17542.
17) R. Abe, K. Shinmei, K. Hara, and B. Ohtani, *Chem. Commun.*, 2009, 3577-3579.
18) M. Tabata, K. Maeda, M. Higashi, D. Lu, T. Takata, R. Abe, and K. Domen, *Langmuir*, 2010, **26**, 9161-9165.
19) Y. Miseki, S. Fujiyoshi, T. Gunji, and K. Sayama, *Catal. Sci. Technol.*, 2013, **3**, 1750-1756.
20) Y. Miseki, H. Kusama, H. Sugihara, and K. Sayama, *J. Phys. Chem. Lett.*, 2010, **1**, 1196-1200.
21) J. R. Darwent and A. Mills, *J. Chem. Soc., Faraday Trans. 2*, 1982, **78**, 359-367.
22) W. Erbs, J. Desilvestro, E. Borgarello, and M. Grätzel, *J. Phys. Chem.*, 1984, **88**, 4001-4006.
23) Y. Miseki, H. Kusama, and K. Sayama, *Chem. Lett.*, 2012, **41**, 1489-1491.
24) S. S. K. Ma, K. Maeda, R. Abe, and K. Domen, *Energy Environ. Sci.* 2012, **5**, 8390-8397.
25) T. Arai, M. Yanagida, Y. Konishi, H. Sugihara, and K. Sayama, *Electrochemistry*, 2008, **76**, 128-131.
26) G. R. Bamwenda, K. Sayama, and H. Arakawa, *J. Photochem. Photobiol. A: Chem.*, 1999, **122**, 175-183.
27) G. R. Bamwenda, T. Uesigi, Y. Abe, K. Sayama, and H. Arakawa, *Appl. Catal. A: General*, 2001, **205**, 117-128.
28) T. Ohno, D. Haga, K. Fujihara, K. Kaizaki, and M. Matsumura, *J. Phys. Chem. B*, 1997, **101**, 6415-6419.
29) A. Iwase, H. Kato, and A. Kudo, *J. Sol. Energy Eng.*, 2010, **132**, 021106.
30) H. Kato, K. Asakura, and A. Kudo, *J. Am. Chem. Soc*., 2003, **125**, 3082-3089.
31) A. Iwase, H. Kato, and A. Kudo, *ChemSusChem*, 2009, **2**, 873-877.
32) H. Kato, Y. Sasaki, A. Iwase, and A. Kudo, *Bull. Chem. Soc. Jpn.*, 2007, **80**, 2457-2564.
33) S. P. Moulik and K. K. S. Gupta, *J. Indian Chem. Soc*., 1972, **49**, 447.
34) R. A. Whiteker and N. Davidson, *J. Am. Chem. Soc*., 1953, **75**, 3081-3085.
35) S. J. Hong, S. Lee, J. S. Jang, and J. S. Lee, *Energy Environ. Sci*., 2011, **4**, 1781-1787.
36) L. Kavan, M. Gratzel, S. E. Gilbert, C. Klemenz, and H. J. Scheel, *J. Am. Chem. Soc*., 1996, **118**, 6716-6723.
37) S. Cheng, B. A. Dempsey, and B. E. Logan, *Environ. Sci. Technol*., 2007, **41**, 8149-8153.
38) H. Eom, K. Chung, I. Kimand, and J. Han, *Chemosphere*, 2011, **85**, 672-676.

